Electronic Supplementary Information

Mineral acid-triggered multicolor room-temperature phosphorescence nanoprobes for time-resolved bioimaging

Zhixia Feng [a]‡, Wenxin Xu [a]‡, Jinpan Zhang [a]‡, Peiling Dai [b], Jiawei Zhang [a], Qiang Zhao [b], Mingyue Cui [a]*, Bin Song [a]*, and Yao He [a, c, d]*

a. Suzhou Key Laboratory of Nanotechnology and Biomedicine, Institute of Functional Nano & Soft Materials & Collaborative Innovation Centre of Suzhou Nano Science and Technology (NANO-CIC), Soochow University, Suzhou 215123, China.

b. State Key Laboratory of Organic Electronics and Information Displays & Jiangsu Key Laboratory for Biosensors, Institute of Advanced Materials (IAM) & Institute of Flexible Electronics (Future Technology), Nanjing University of Posts & Telecommunications, Nanjing 210023, China.

c. Macao Translational Medicine Center, Macau University of Science and Technology, Taipa 999078, Macau SAR, China

d. Macao Institute of Materials Science and Engineering, Macau University of Science and Technology, Taipa 999078, Macau SAR, China

* E-mail: mingyuecui@suda.edu.cn; bsong@suda.edu.cn; yaohe@suda.edu.cn

‡ Zhixia Feng, Wenxin Xu, Jinpan Zhang contributed equally to this work.

1. Experimental section

1.1 Materials.

Materials: (3-Aminopropyl) trimethoxysilane (APTMS, 97%) was purchased from Sigma-Aldrich. Boric acid (Mw = 61.83, ≥99%) was purchased from Shanghai Aladdin Biochemical Technology Co., Ltd. Phosphoric acid (85%) was purchased from Beijing Chemical Reagent Company (Beijing, China). CellTracke™ Red CMTPX (CMTPX) was obtained from Yeasen Biotech Co., Ltd. (Shanghai, China). Hoechst 33342 was obtained from Solarbio. CCK8 reagent was obtained from MCE. Deionized water from the Milli-Q water purification system was used throughout the experiments. All chemicals used were of analytical reagent grade and used without any further purification.

1.2 Characterization.

TEM/HRTEM images were taken through a Talos 200X electron microscope operated at 200 kV and analyzed through ImageJ software. High-resolution X-ray photoelectron spectroscopy (XPS) images were collected on a Kratos AXIS UltraDLD ultrahigh vacuum (UHV) surface analysis system. All the data were collected in transmission mode at ambient temperature. Photoluminescence (PL) measurements were performed with a HITACHI F-4700 (Tokyo, Japan) fluorescence spectrofluorometer. Time-resolved phosphorescence emission spectra were recorded in a transient spectrum system on an Edinburgh FLS 1000 spectrofluorometer. The dynamics of the emission decays were monitored by using the FLS1000 time-resolved single-photon counting multichannel scaling (MCS) mode with data collection for 10000 counts. Time-resolved fluorescence decay curves were obtained on a HORIB-FM-2015 spectrofluorometer with 370 nm lasers as the excitation source. The dynamic light scattering (DLS) was performed using a MALVERN ZEN3690. Ultraviolet-visible (UV-Vis) absorption spectra were measured on a PerkinElmer Lambda 950 spectrometer. Absolute quantum yields in the solid phase and in the aqueous phase were tested at room temperature using an absolute quantum yield measurement system (Hamamatsu, Japan).

1.3 Synthesis of SiB*m*.

First, 2.0 mL of APTMS solution was dissolved in 20 mL of deionized water, and then, boric acid (m = 2.0, 2.5, 3.0 g) was added to the aqueous solution and stirred for 30 min. The resulting transparent solution was heated in a microwave oven (750 W) for 3 min and subsequently cooled to room temperature naturally. The white solid (SiB*m*) was obtained.

1.4 Synthesis of SiB*m*P*n*.

First, 2 g of SiB*2.5* (m = 2.5 g) aqueous solution and phosphoric acid (n = 0.5, 1.0, 2.0 mL) were dispersed in 15 mL of deionized water with stirring for 15 min. Then, the resulting transparent solution was heated in the microwave oven (750 W) for 2 min and cooled to room temperature naturally. The SiB*2*.5P*n* was obtained.

1.5 Computational details.

Theoretical calculations of the complexation energy, excitation energies, natural transition orbitals (NTOs) and corresponding spin-orbit coupling (SOC) constants of hydrolyzed silane, SiB*m*, and SiB*m*P*n* were carried out based on the wavefunction-based quantum chemistry technique of symmetry-adapted perturbation theory (SAPT) coupled with the basis set of jun-cc-pVDZ, and time-dependent density functional theory (TD-DFT) and spin-orbit coupling were carried out at the B3LYP/def2-TZVP (D3) level with the RIJCOSX tool using the ORCA software package.

1.6 Cell co-localization experiments.

In order to investigate whether the SiB2.5P1 probe could enter the cells for imaging analysis, the SiB*2.5*P*1* probe (100 μg/mL) was co-incubated with cancer cells U87 for 12 h, then washed with PBS (pH: 7.4) three times, and then incubated with the cytoplasmic dye (CellTrace™ Red CMTPX) (100 μg/mL) in the petri dish for 2 h, and then washed three times with PBS (pH: 7.4). Finally, cell imaging images were acquired by confocal microscopy with an excitation wavelength of 405 nm, and images corresponding to the emission spectra of SiB2.5P1 probe at 425-460 nm were acquired with 588 nm excitation, and fluorescence at 600-633 nm was received. The acquired fluorescence images were processed with ImageJ 1.54d, and the fluorescence intensity distribution maps and co-localization coefficients (Rr) were calculated based on the following formulae:

$$Rr = \frac{\sum (I1 - \bar{I}1)(I2 - \bar{I}2)}{\sqrt{\sum (I1 - \bar{I}1)^2 \sum (I2 - \bar{I}2)^2}}$$

1.7 Cellular imaging at various incubation times.

To examine the influence of incubation time on cellular imaging, U87 cells were incubated with the SiB*2.5*P*1* probe at a concentration of 100 μg/mL for 2, 6, and 12 hours, respectively. Following incubation, the cells were washed three times with PBS (pH 7.4) to remove excess probe. Subsequently, cell imaging was performed using confocal microscopy with excitation at a 405 nm laser and emission captured within the ranges of 420-460 nm, 488-515 nm, and 545-580 nm. Fluorescence signal intensities were then quantified from the resulting images using ImageJ software version 1.54d.

1.8 Optical stability assessment.

To investigate the optical stability of SiB*2.5*P*1* in cell imaging, the SiB*2.5*P*1* probe (100 μg/mL) was first incubated with U87 cancer cells for 12 hours. The cells were then washed three times with PBS (pH: 7.4), after which the nuclear dye Hoechst (100 μg/mL) was added to the culture dish and the cells were incubated for an additional 2 hours. Following another three washes with PBS (pH: 7.4), the cells were subjected to continuous illumination with a 405 nm laser for durations of 0, 5, 15, 30, 60, and 90 minutes. Cell images were captured through Zeiss laser scanning microscope (Zeiss LSM800). Optical signals were collected at wavelengths of 420-460, 488-515, and 545-580 nm, respectively. The collected images were analyzed for fluorescence signal intensity using ImageJ 1.54d, and the data were processed and plotted using Origin.

1.9 Cytotoxicity assessment.

To evaluate the cytotoxicity of SiB*2.5*P*1*, U87 (i.e., a human glioma cell line) and HBMEc (i.e., human brain microvascular endothelial cells) cells were plated in 96-well plates at a density of 10^4 cells per well and incubated for 12 h. Then, the old medium was replaced with fresh medium containing SiB*2.5*P*1* at various concentrations (100 μL per well, 0-1000 μg/mL). The cells were treated with the materials for 1, 3, 6, 12, 24 or 48 h at 37°C, and the cytotoxicity was evaluated

through the use of CCK8 reagent. Briefly, the drug-treated cells were washed twice with PBS and mixed with reaction solution containing CCK8. After incubating at 37 °C for 1.5 h, the A450 values were read by a microplate reader (Thermo Fisher Scientific).

1.10 Phosphorescence lifetime imaging microscope cell imaging.

U87 cells were cultured with 100 μg/mL SiB*2.5*P*1* for 12 h. After incubation, the cells were washed with PBS (pH 7.4) three times. The labeled cells were mounted on slides in fluoromount (Sigma, F4680) with coverslips. Then, phosphorescence cell images were captured through a phosphorescence lifetime imaging microscope (PLIM). The PLIM image setup was integrated with an Olympus IX81 laser scanning confocal microscope. The phosphorescence signals were detected by confocal microscopy, and correlative calculations of the data were performed with professional software provided by the PicoQuant Company. The light from the pulse diode laser head (Pico Quant, PDL 800-D) with an excitation wavelength of 405 nm and a frequency of 1 MHz (> 1 ms) was focused onto the sample with a 40×/NA 0.95 objective lens for single-photon excitation. The PLIM data were processed in SymPhoTime 64 PRO software (Pico Quant Company) and exported in ASCII (line profiles) or BMP (images) format. PLIM data obtained from 256 × 256 regions of interest were fit using double exponential tailfit and a binning factor of 1 in SymPhoTime 64pro software.

Calculation details of above-mentioned SBR values have been provided as follow. Particularly, the samples with or without RTP probes treatment are firstly employed as background or signal groups, respectively. Then, the intensity of background (Ib.) and signal (Is.) in resultant images is analyzed by ImageJ 1.52 software. After six parallel experiments, the SBR values could be calculated as the ratio between the average values of Is. and Ib.[1]

1.11 Statistical analysis.

For statistical significance testing, we used one-way ANOVA or paired two-tailed t tests (** indicates $p < 0.01$, *** indicates $p < 0.001$, ns indicates no significance). The statistical analysis was performed by using GraphPad Prism software. Error bars represent the standard deviation obtained from three independent measurements. All imaging experiments were repeated three times with similar results.

2. Supplementary Tables and Figures

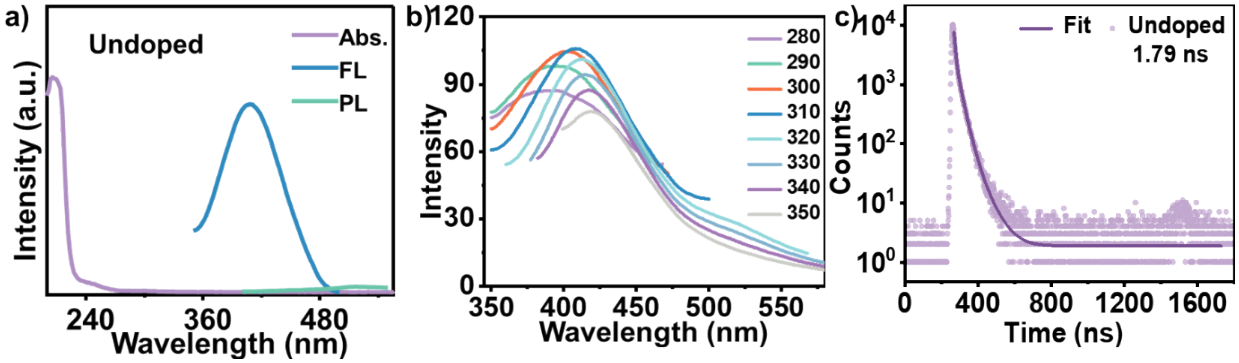

Figure S1. The normalized UV–visible, fluorescence, and phosphorescence spectra (a); fluorescence emission spectra under serial excitation wavelengths from 280 to 350 nm (b); and fluorescence lifetime decay curves (λ_{ex} = 300 nm) (c) of the undoped material.

In Figure S1 (a) and (b), the maximum emission wavelength of the undoped material is ~408 nm (λ_{ex} = 310 nm), and no phosphorescence emission is observed from the undoped material. The time-resolved fluorescence-decay curve is fitted to a triexponential function, and the average fluorescence lifetime of the undoped material is calculated to be 1.79 ns (Figure S1c).[2]

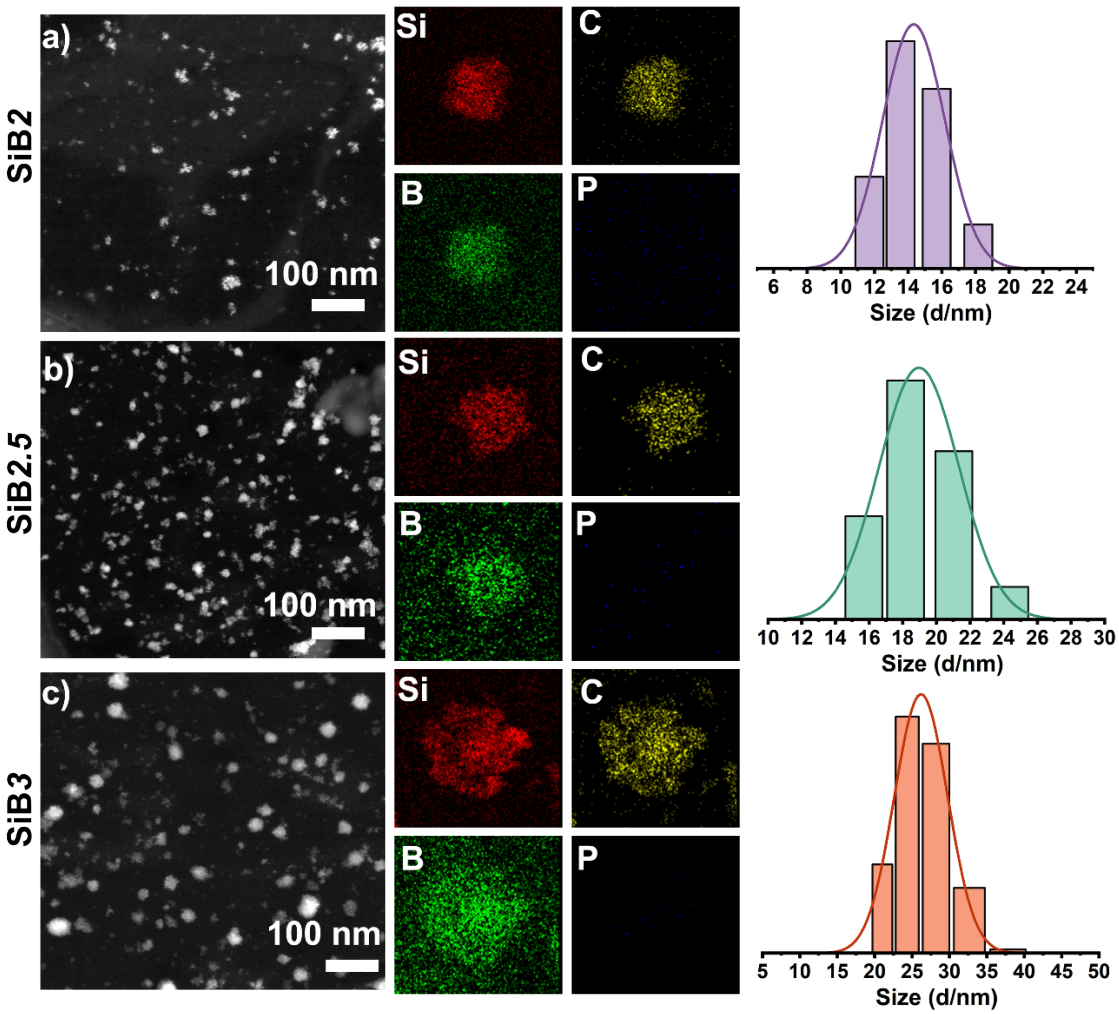

Figure S2. (a-c) STEM images, EDS and DLS particle size profiles of SiB*m* with different boric acid doping concentrations.

To determine the structure of the SiB*m*, the morphologies are imaged by scanning transmission electron microscopy (STEM). As shown in Figure S2, the resultant SiB*m* particles are uniform in size and exhibit an aggregated irregular shape. It is clear that the size of the SiB*m* increases from about 10 nm to approximately 30 nm with increasing dopant concentration. The above results are attributed to mineral acid-induced aggregation. In addition, energy dispersive spectroscopy (EDS) mapping is used to characterize the distribution of elements in the as-prepared SiB*m*. In brief, Si, C, and B are clearly detected in the SiB*m*.

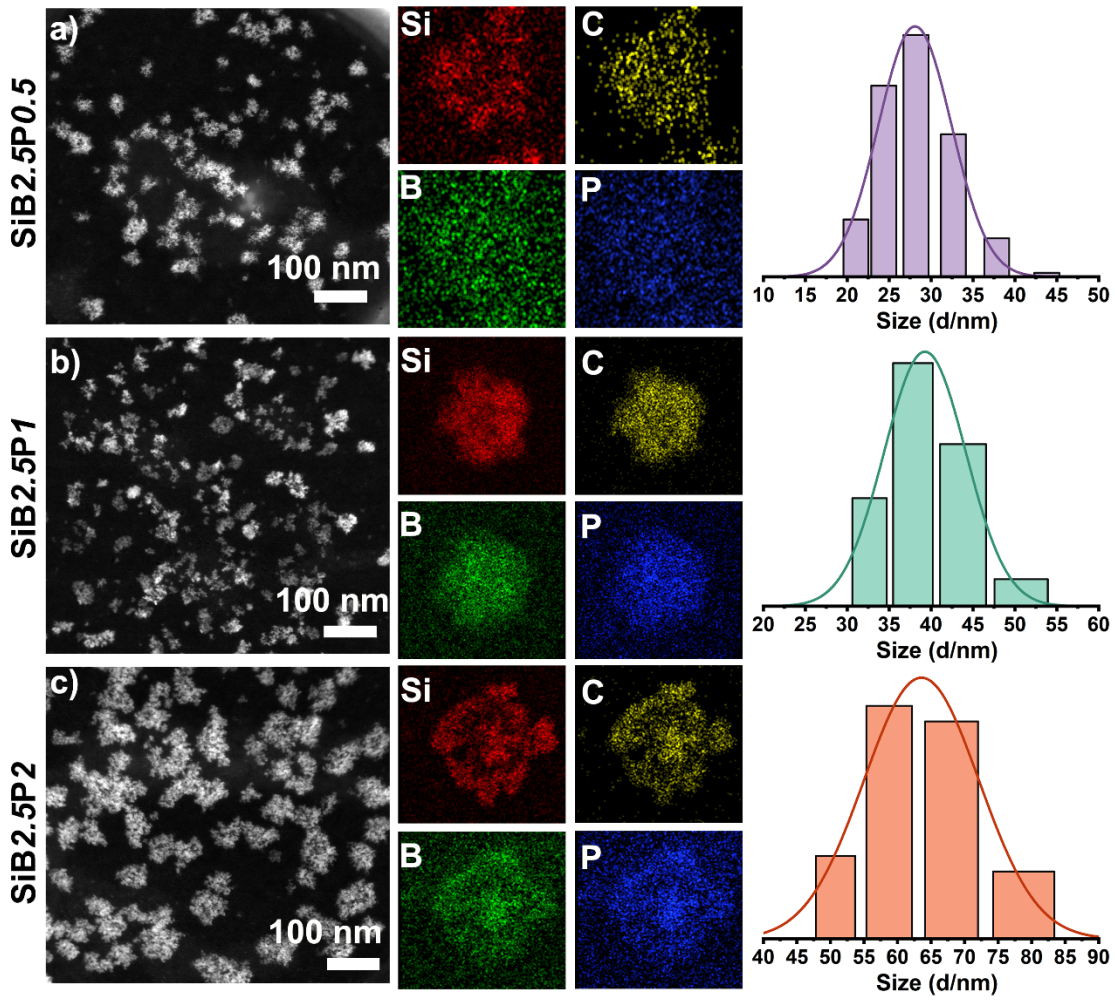

Figure S3. (a-c) STEM images, EDS and DLS particle size profiles of SiB*m*P*n* with different phosphate doping concentrations.

As shown in Figure S3, the resultant SiB*m*P*n* particles are uniform in size and exhibit an aggregated irregular shape. It is clear that the size of the SiB*m*P*n* increases from about 30 nm to approximately 80 nm with increasing dopant concentration. The above results are attributed to mineral acid-induced aggregation. Therefore, the size of the SiB*m*P*n* can be finely controlled by simply tuning the chemical composition. In addition, energy dispersive spectroscopy (EDS) mapping is used to characterize the distribution of elements in the as-prepared SiB*m*P*n*. In brief, Si, C, B, and P are clearly detected in SiB*m*P*n* systems.

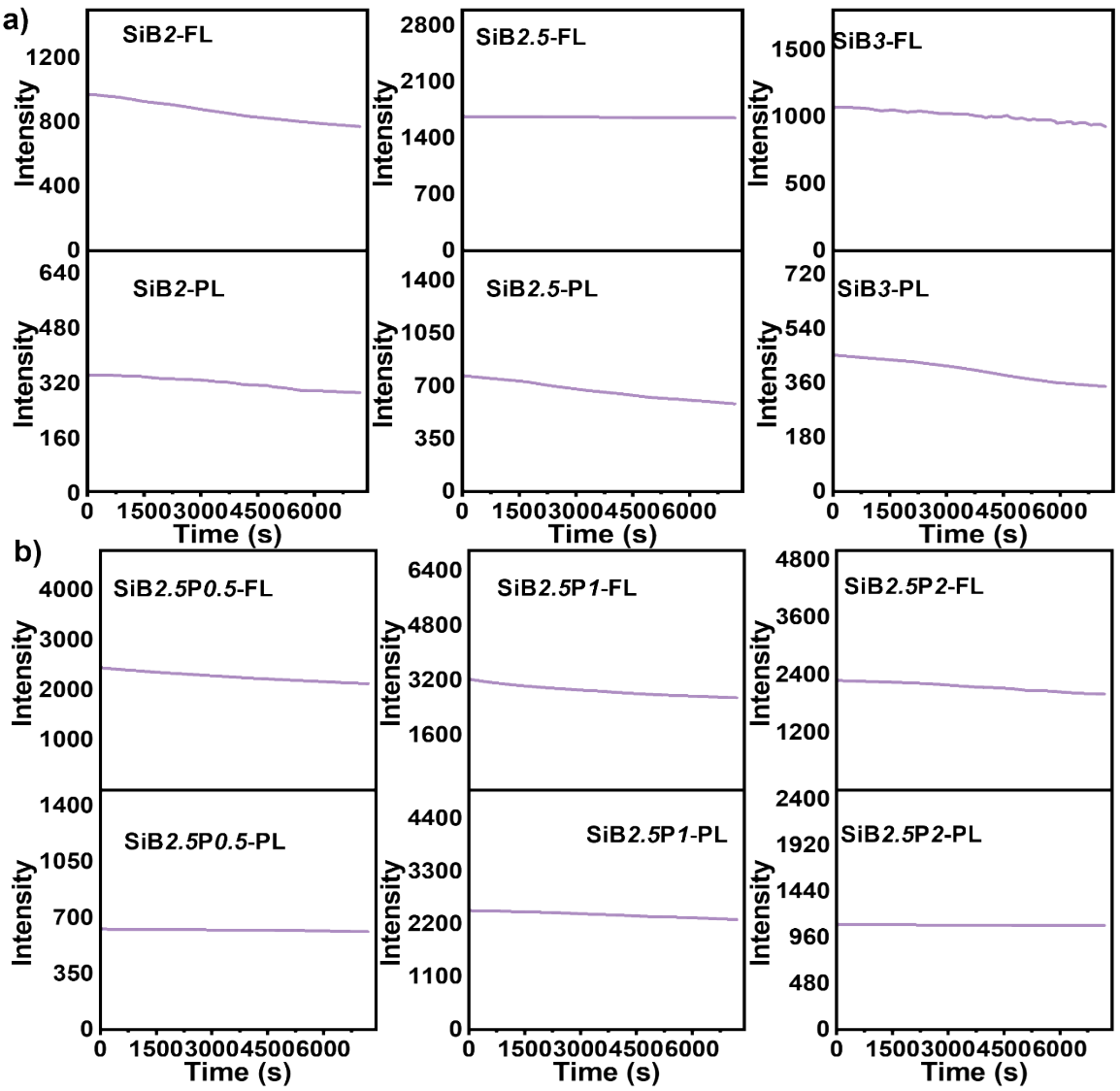

Figure S4. FL and PL intensities spectra of SiB*m* (a) and SiB*m*P*n* (b) in aqueous solution during 2-h UV irradiation (λ_{ex} = 350 nm).

As represented in Figure S4, after two hours of UV radiation, the fluorescence and phosphorescence intensities of SiB*m* and SiB*m*P*n* are maintained at more than 76% of the corresponding maximum values, demonstrating their excellent stability.

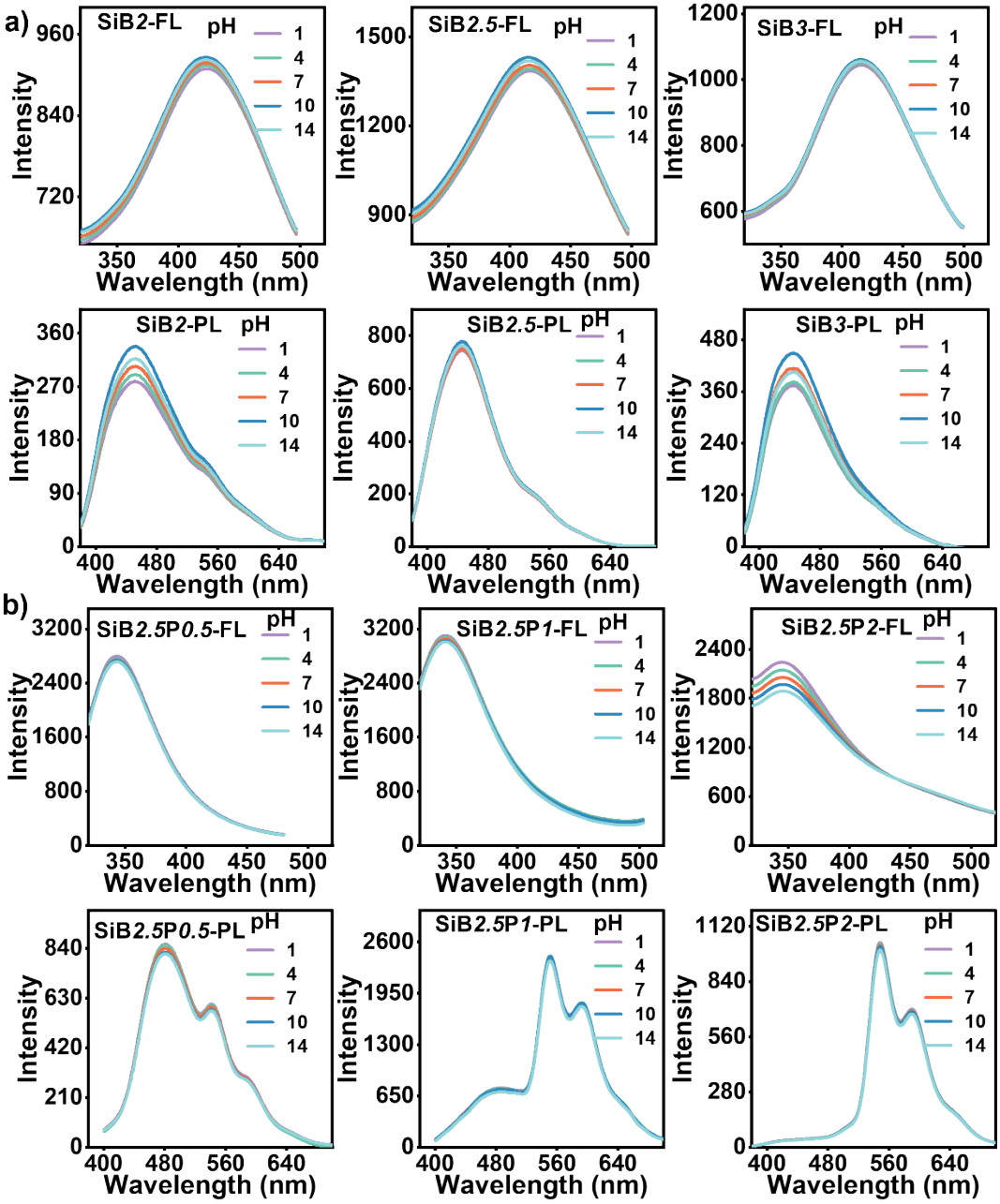

Figure S5. FL and PL intensities spectra of SiB*m* (a) (λ_{ex} = 340 and 350 nm) and SiB*m*P*n* (b) (λ_{ex} = 280 and 350 nm), respectively, in aqueous solution under different acid-base environments.

As illustrated in Figure S5, the fluorescence and phosphorescence intensities of SiB*m* and SiB*m*P*n* are maintained at more than 82% of the corresponding initial luminescence intensities in different acid-base environments.

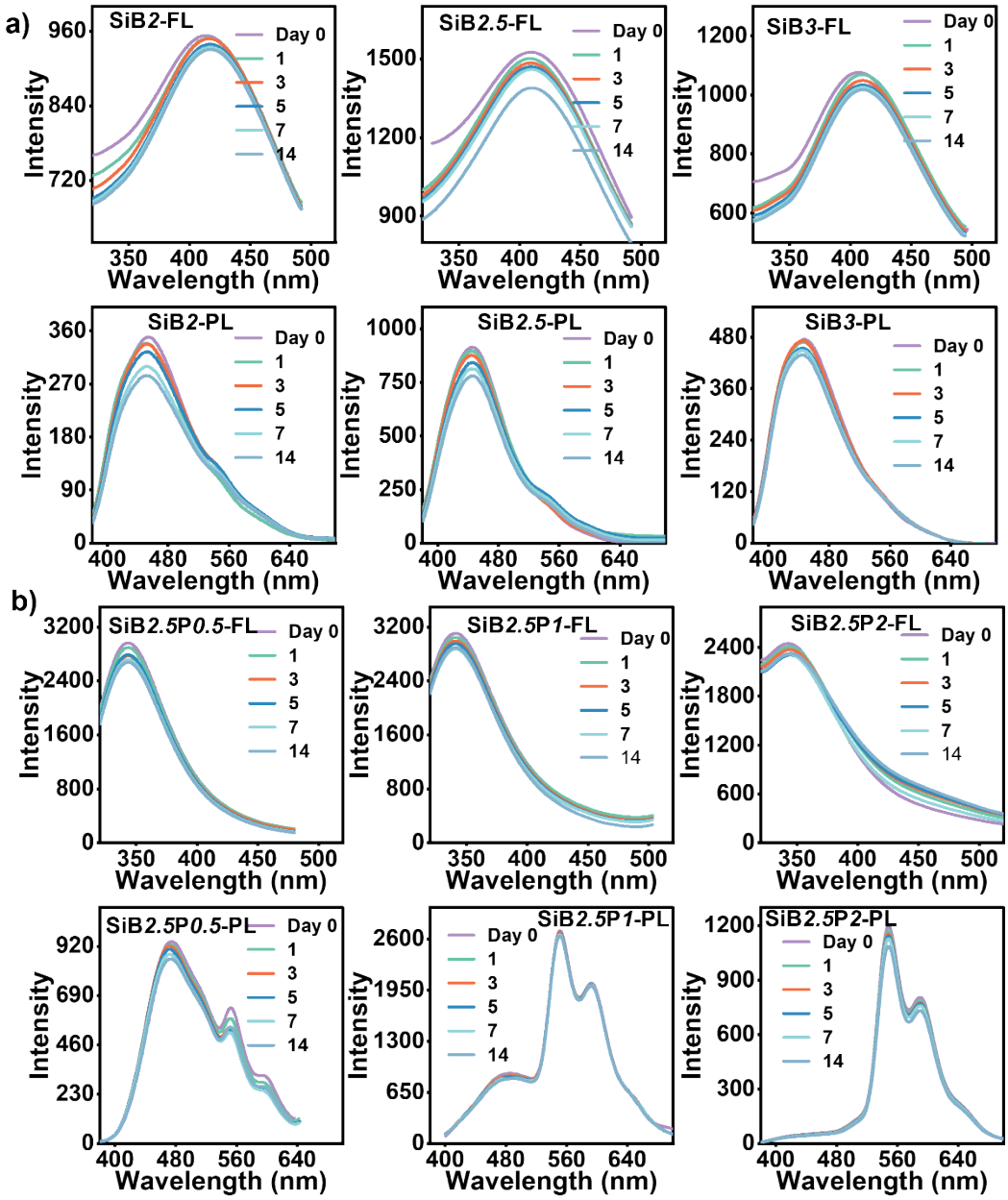

Figure S6. FL and PL intensities spectra of SiB*m* (a) (λ_{ex} = 340 and 350 nm) and SiB*m*P*n* (b) (λ_{ex} = 280 and 350 nm), respectively, in aqueous solution during 14-day storage.

In Figure S6, the fluorescence and phosphorescence intensities of SiB*m* and SiB*m*P*n* illustrate excellent storage stability and maintain more than 81% of the corresponding maximum luminescence intensities during 14-day storage.

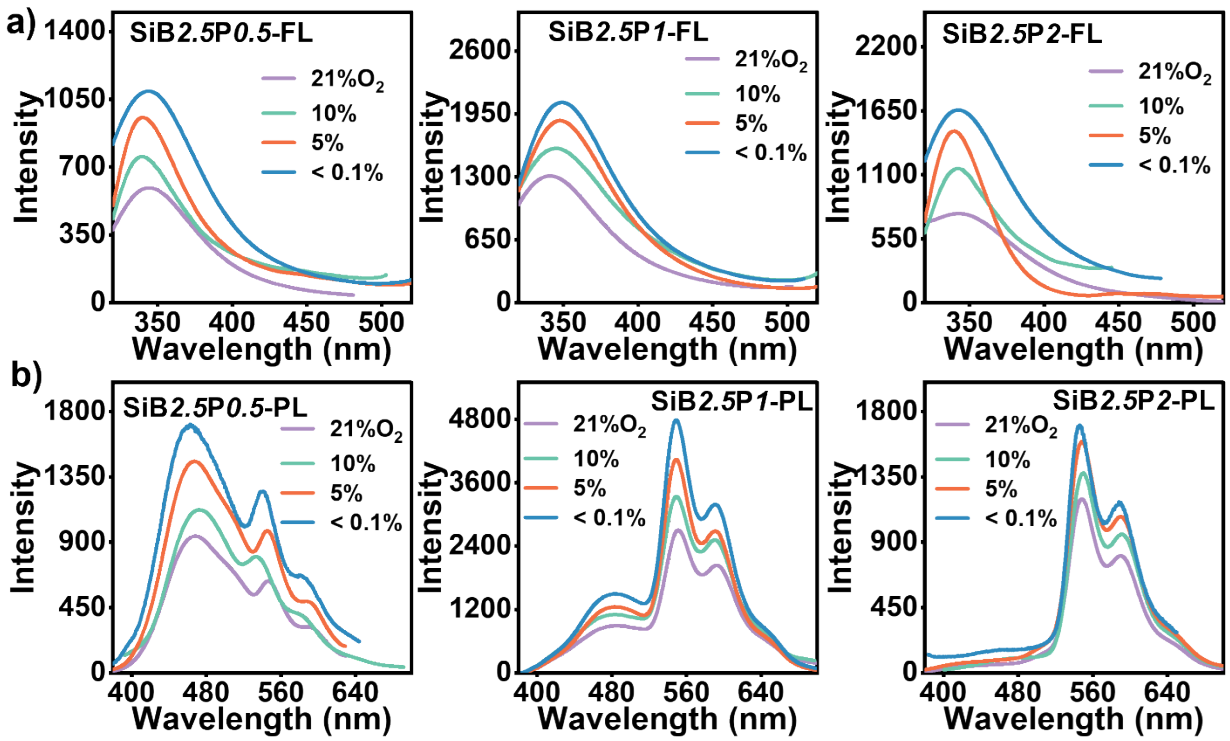

Figure S7. (a) FL (λ_{ex} = 280 nm) and (b) PL (λ_{ex} = 350 nm) intensities spectra of SiB*m*P*n* in aqueous solution at different oxygen concentrations.

As shown in Figure S7, both fluorescence and phosphorescence intensity of SiB*m*P*n* increase with decreasing oxygen concentration. With the decreased oxygen concentrations (from <0.1% to 21%), the intensities of FL and PL can be remarkably strengthened.

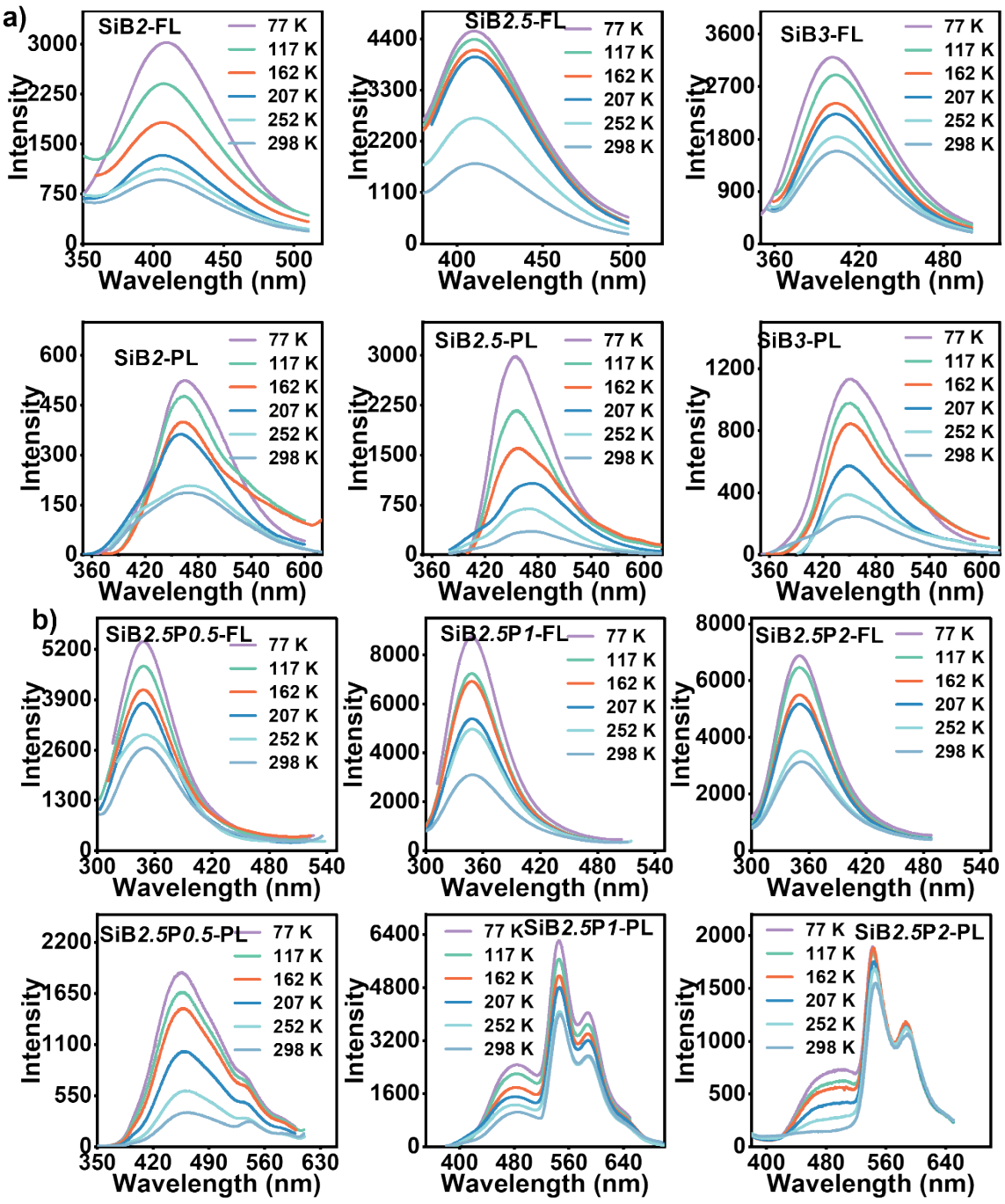

Figure S8. FL and PL intensities spectra of SiB*m* (a) (λ_{ex} = 340 and 350 nm) and SiB*m*P*n* (b) (λ_{ex} = 280 and 350 nm) in aqueous solution at different temperatures, respectively.

SiB*m* and SiB*m*P*n* exhibit enhanced FL and PL intensities in low temperature because of the heat-induced quenching effect.

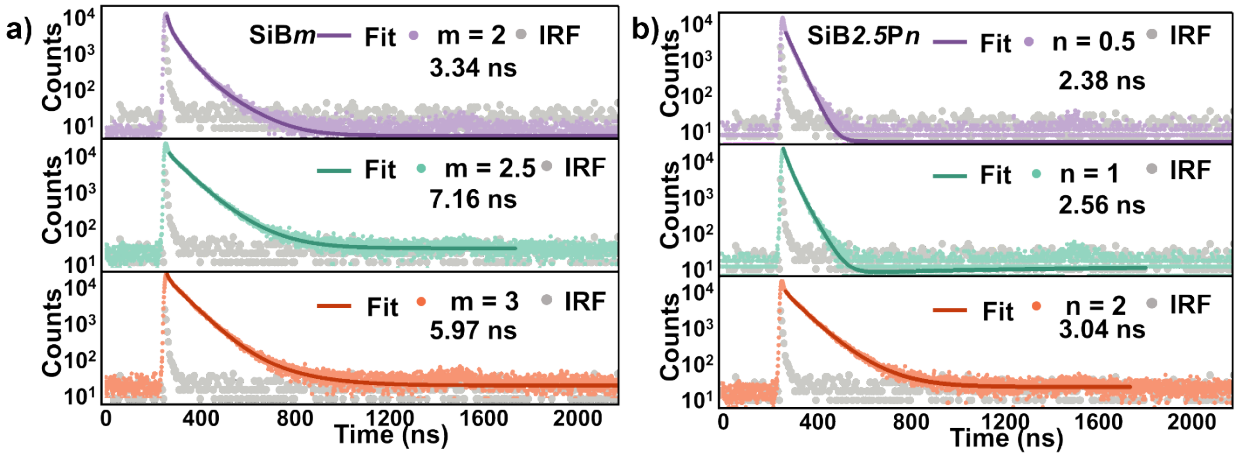

Figure S9. Fluorescence lifetime decay curves of solid powders SiB*m* (a) and SiB*2*.5P*n* (b).

As shown in Figure S9, their time-resolved fluorescence-decay curves are fitted to a triexponential function, and their average fluorescence lifetimes are calculated to be 3.34 ns (m = 2), 7.16 ns (m = 2.5), 5.97 ns (m = 3), 2.38 ns (n = 0.5), 2.56 ns (n = 1) and 3.04 ns (n = 2), respectively.

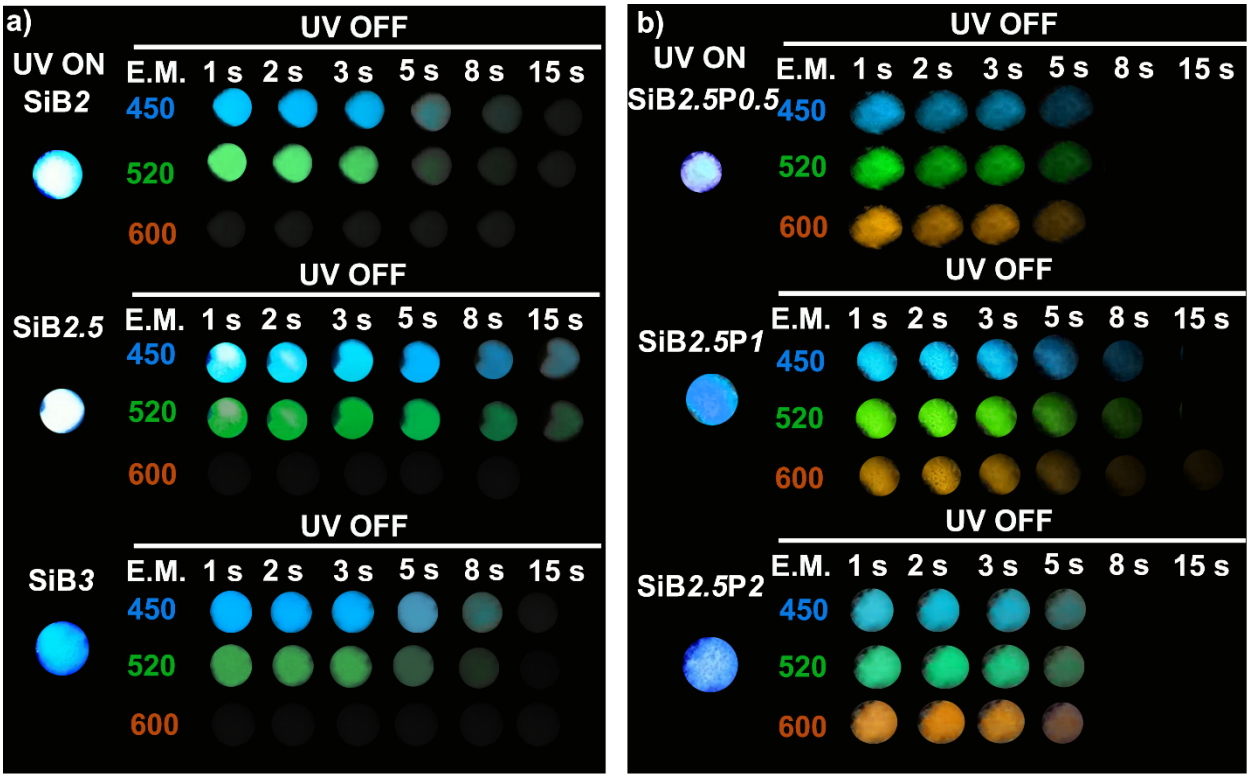

Figure S10. The luminescence photographs of SiB*m* (a) with different boric acid doping concentrations and SiB*m*P*n* (b) with different phosphoric acid doping concentrations under 365 nm UV excitation.

All the samples exhibit greenish-blue fluorescence upon 365 nm UV irradiation. After switching off the UV lamp, the luminescent signals of SiB*m* and SiB*m*P*n* are captured using 450 nm, 520 nm and 600 nm filter, respectively.[3] Compared to those of undoped organic silicon, long-lived RTPs at 450 and 520 nm are observed under UV-off conditions in all the SiB*m* groups. The afterglow time of the SiB*m* ranged from 1 to 15 s and are determined by a digital camera. Among them, SiB*2.5*, which has optimal RTP properties, is used for further construction of dual-doping systems. After the introduction of P, multicolor RTP emission originating at ~450, 520 and 600 nm is observed from SiB*m*P*n* by the naked eye during the 5 s decay process.

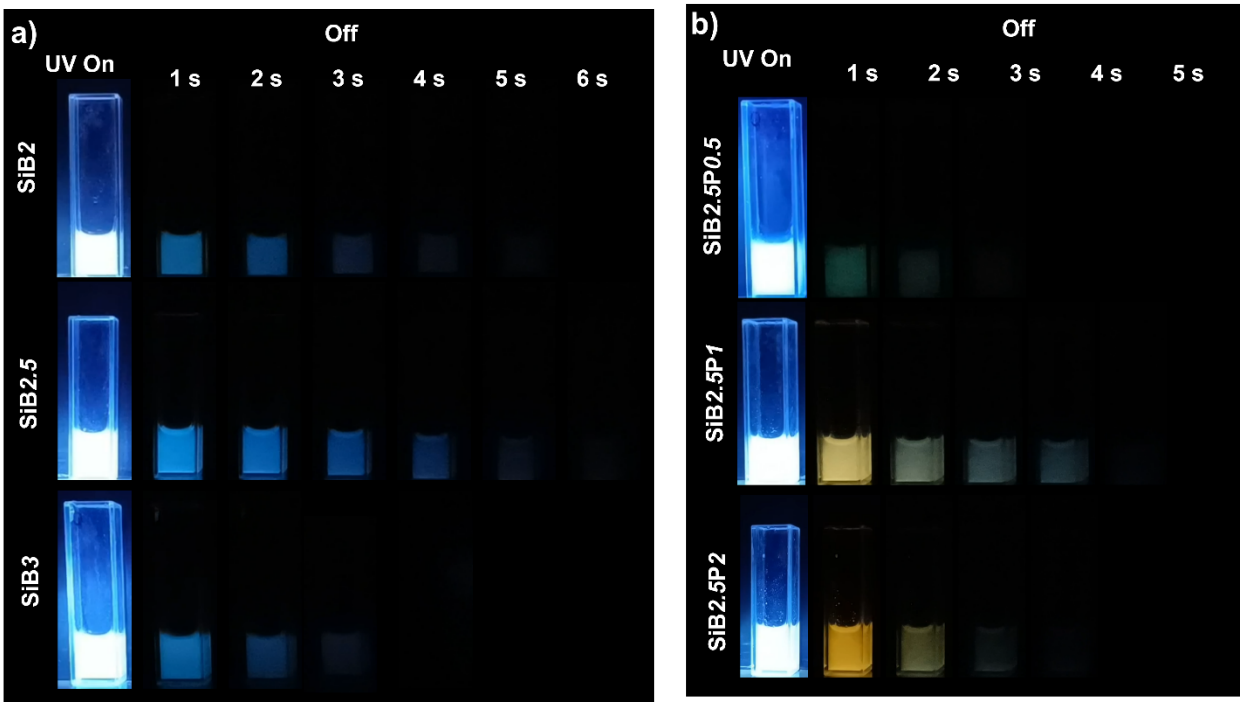

Figure S11. The luminescence photographs of SiB*m* (a) and SiB*m*P*n* (b) in aqueous solution under 365 nm UV excitation.

the SiB*m*P*n* produce long-lived afterglow with multi-color emission in water during 4 s decay time.

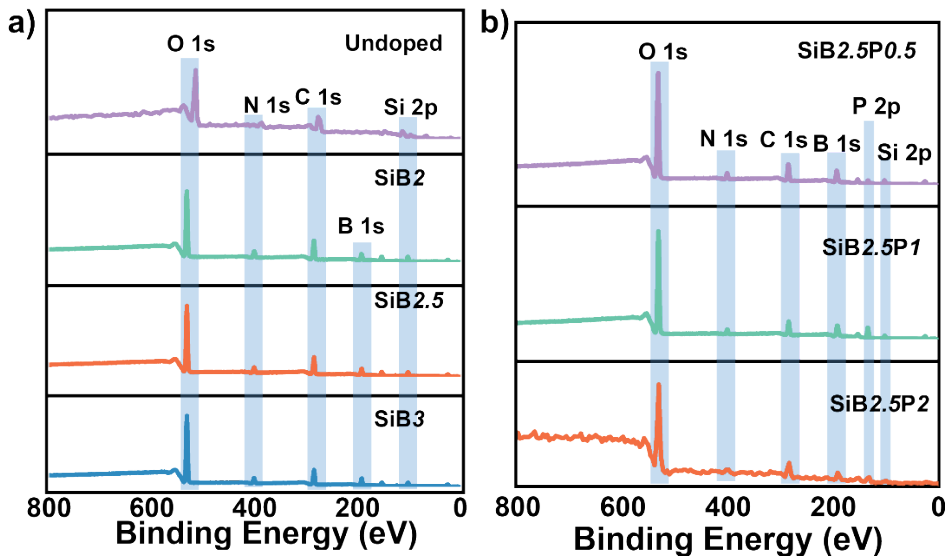

Figure S12. (a) XPS spectra of undoped, SiB*2*, SiB*2*.5, and SiB*3*. (b) XPS spectra of SiB*2*.5P*0.5*, SiB*2.5*P*1* and SiB*2*.5P*2*.

In Figure S12, for the XPS spectra of SiB*2*, SiB*2*.5, and SiB*3*, distinct peaks are observed at approximately 103 eV (Si 2p), 192 eV (B 1s), 285 eV (C 1s), 401 eV (N 1s) and 532 eV (O 1s), demonstrating the presence of Si, B, C, N and O in SiB*2*, SiB*2*.5, and SiB*3*. XPS spectra reveal the presence of C, N, O, Si, B and P (135 eV (P 2p)) in SiB*2*.5P*0.5*, SiB*2.5*P*1* and SiB*2*.5P*2*, respectively.

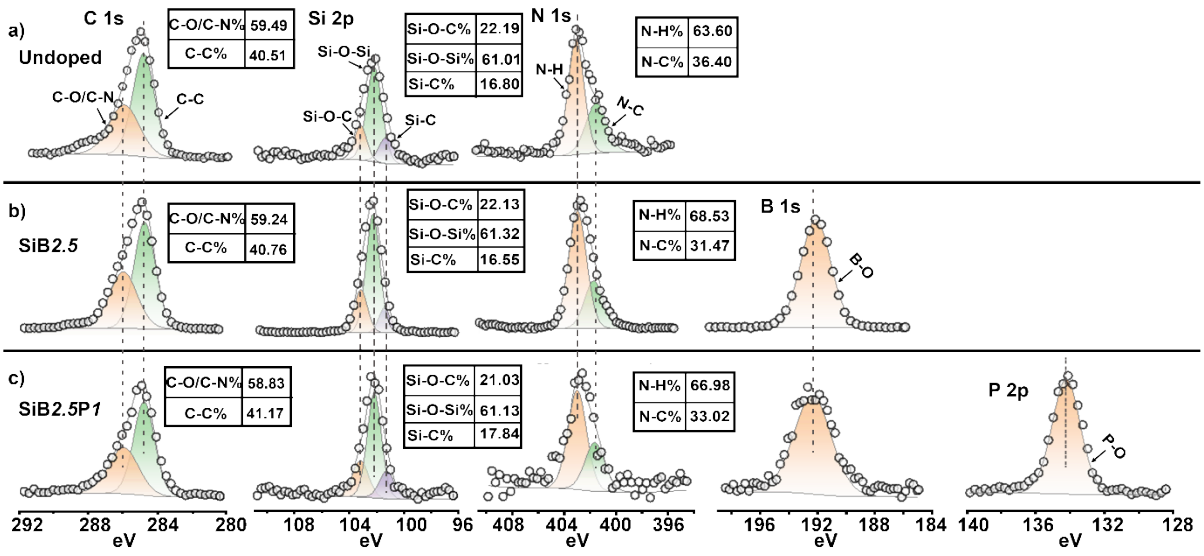

Figure S13. (a) High-resolution XPS spectra of C 1s, Si 2p and N 1s for the undoped group. (b) High-resolution XPS spectra of C 1s, Si 2p, N 1s and B 1s for SiB*2.5*. (c) High-resolution XPS spectra of C 1s, Si 2p, N 1s, B 1s and P 2p for SiB*2.5*P*1* and the corresponding fitting result

The high-resolution XPS (HRXPS) spectrum (Figure S9) of C 1s exhibited two components, C−C (284.7 eV) and C−O/C−N (286.1 eV). HRXPS of the Si 2p spectrum reveals three peaks, which are attributed to Si−O−C (103.3 eV), Si−O−Si (102.4 eV), and Si−C (101.5 eV). Two peaks located at 400.8 and 402.7 eV are observed in the high-resolution N 1s spectrum of SiB*2.5*P*1*, corresponding to N−C and N−H, respectively. The high-resolution B 1s and P 2p spectra of SiB*2.5*P*1* can be fitted to one peak centered at 192.2 and 134.1 eV, originating from B−O and P−O bonds, respectively.[4]

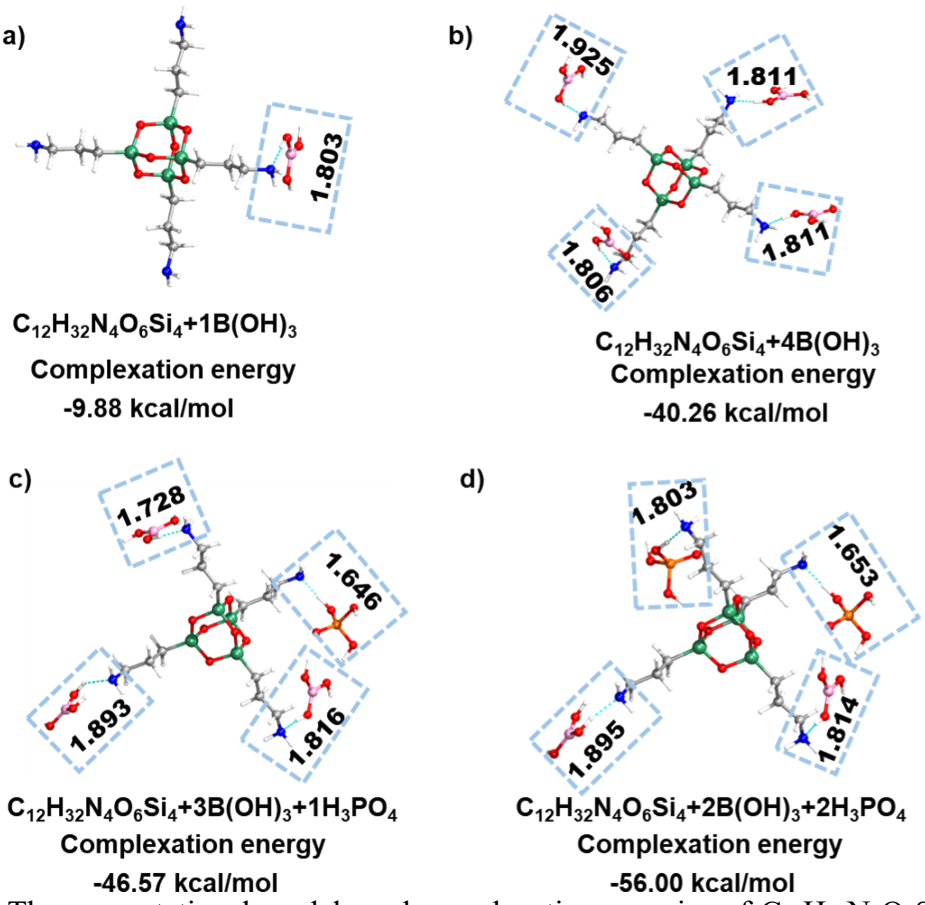

Figure S14. The computational models and complexation energies of $C_{12}H_{32}N_4O_6Si_4$+1B(OH)$_3$ (a), $C_{12}H_{32}N_4O_6Si_4$+4B(OH)$_3$ (b), $C_{12}H_{32}N_4O_6Si_4$+3B(OH)$_3$+1H_3PO_4 (c) and $C_{12}H_{32}N_4O_6Si_4$+2B(OH)$_3$+2H_3PO_4 (d) dopants.

The total complexation energy can be naturally decomposed into physically meaningful energy components of electrostatics, induction, dispersion, and exchange by SAPT calculations. The total complexation energies of the $C_{12}H_{32}N_4O_6Si_4$+1B(OH)$_3$, $C_{12}H_{32}N_4O_6Si_4$+4B(OH)$_3$, $C_{12}H_{32}N_4O_6Si_4$+3B(OH)$_3$+1H_3PO_4 and $C_{12}H_{32}N_4O_6Si_4$+2B(OH)$_3$+2H_3PO_4 dopants were determined to be -9.88, -40.26, -46.57 and -56.00 kcal/mol, respectively. It should be noted that adjustable complexation energies can ultimately affect the strength of intermolecular interactions between materials, thus giving rise to a significant influence on the RTP properties.[5]

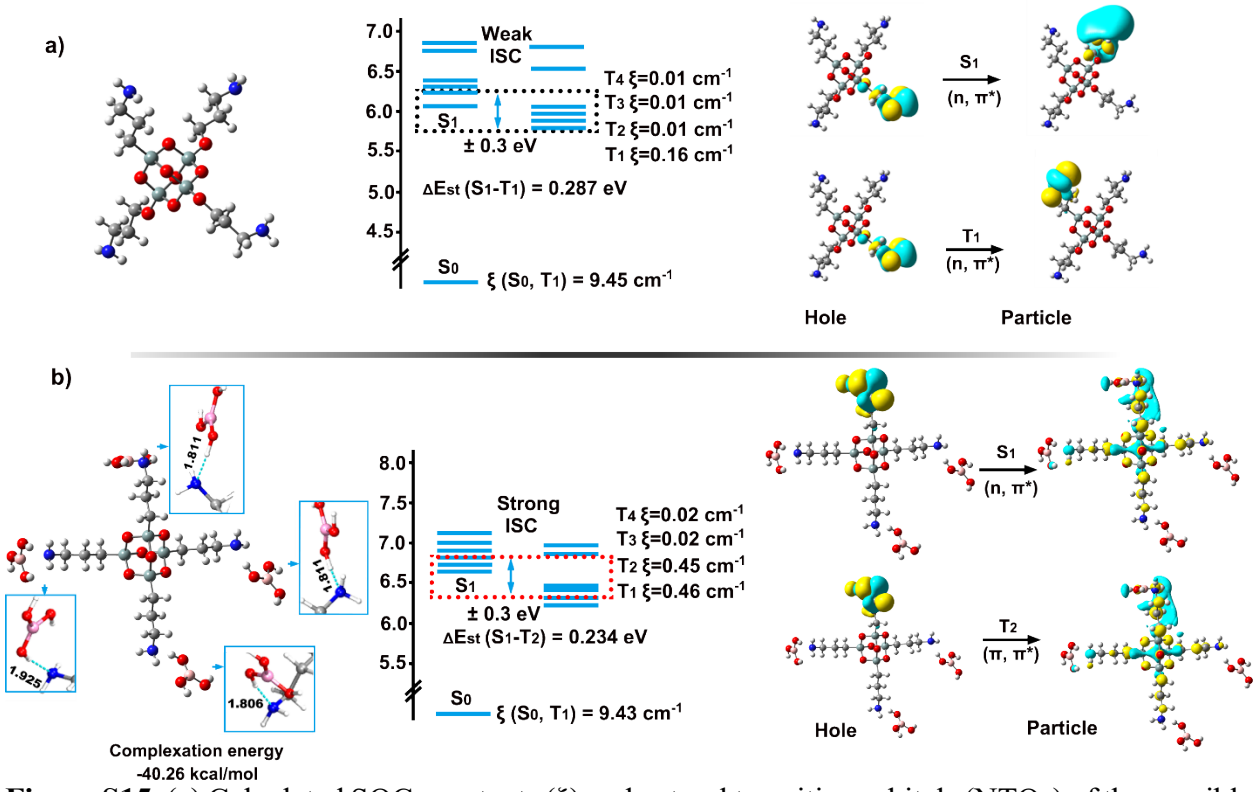

Figure S15. (a) Calculated SOC constants (ξ) and natural transition orbitals (NTOs) of the possible complex in hydrolyzed silane. Diagrams of the calculated complexation energy, the SOC constants between the singlet and triplet excited states, and the NTO characteristics of the possible complex in SiB*m* (b).

To gain further insight into the luminous mechanism of these systems, the excited-state energy is also studied in detail. In the $C_{12}H_{32}N_4O_6Si_4$ group, there are four possible ISC channels from S1 to Tn (S_1-T_1, T_2, T_3, T_4) ($\Delta Est \leq \pm 0.3$ eV), and the corresponding spin-orbit coupling (SOC) constants (ξ) are 0.16, 0.01, 0.01 and 0.01 cm^{-1}, respectively, indicating that the ISC process is insufficient for RTP.[6] After complexation with boric acid and phosphoric acid, the enhanced SOC constants (S_1 to T_n (S_1-T_1, T_2, T_3, T_4)) demonstrate an efficient ISC process. In addition, the corresponding SOC from S1 to Tn (S_1-T_1, T_2, T_3, T_4) for $C_{12}H_{32}N_4O_6Si_4$+4B(OH)$_3$ are 0.46, 0.45, 0.02 and 0.02 cm^{-1}. The NTO data shows that after boric acid doping, localized excited states exist in the $C_{12}H_{32}N_4O_6Si_4$ system, and the transition changes from (n, π*) in the S1 state to (π, π*) in the T_1 state.[7] Thus, ISC can occur from the (n, π*) S1 to (π, π*) T_2 excited states accompanied by increased SOC constants (from 0.16 to 0.45 cm^{-1}) and decreased ΔEst (from 0.287 to 0.234 eV), promoting effective RTP emission in $C_{12}H_{32}N_4O_6Si_4$+4B(OH)$_3$.

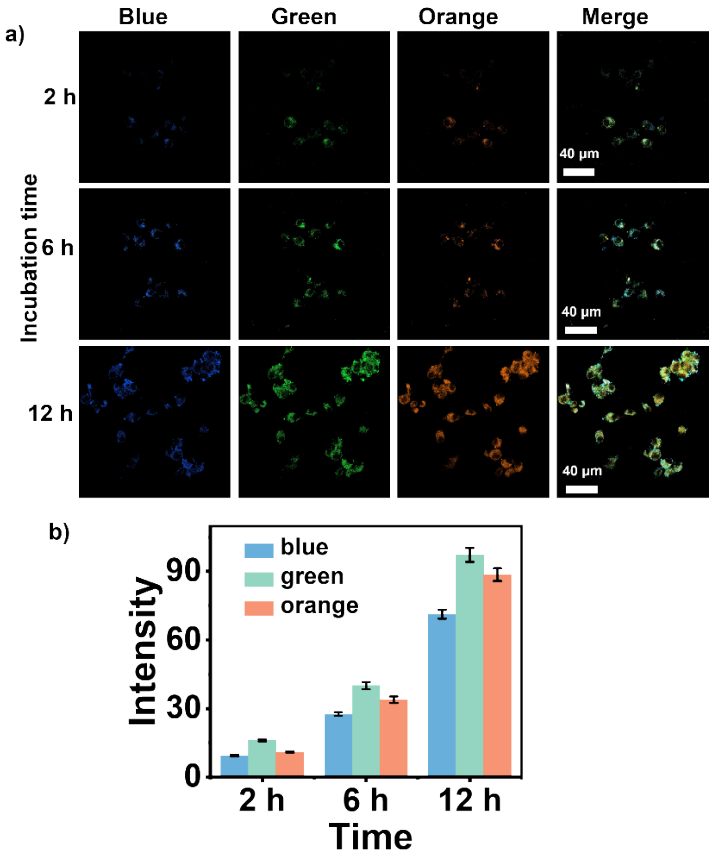

Figure S16. Cellular imaging (a) and luminescence intensity statistics (b) at different times of U87 cells incubated with SiB*2.5*P*1* (100 μg/mL).

As displayed in Figure S16a, the SiB*2.5*P*1* was incubated with U87 cells for 2, 6, and 12 hours, respectively. Apparently, the intensities from blue, green and orange signals increase with prolonging the co-incubation time from 2 to 12 hours.

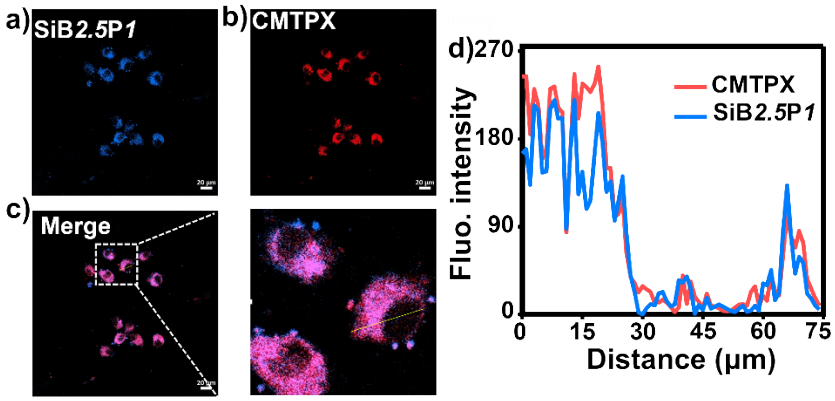

Figure S17. Laser scanning confocal microscopy images of U87 cells incubated with SiB*2.5*P*1* (100 μg/mL) (a), CellTrace™ Red CMTPX (a red fluorescent dye for the cytoplasm) (b), and merge (c). Scale bar: 20 μm. (d) Colocalization analyses of SiB*2.5*P*1* and CMTPX are shown in (c).

To further investigate the intracellular distribution of these nanoprobes, U87 cells treated with SiB*2.5*P*1* were stained with CellTrace™ Red CMTPX (a red fluorescent dye for the cytoplasm). As shown in Figure S17a-c, the strong blue emission signal in the fluorescence image of SiB*2.5*P*1* under 405 nm laser excitation and the red and blue fluorescence signals well overlap in the cytoplasm, the as-prepared RTP nanoprobes (i.e., SiB*2.5*P*1*) mainly distribute in the cytoplasm. The Pearson's colocalization coefficient (Rr) is calculated as 94% (Figure S17d).

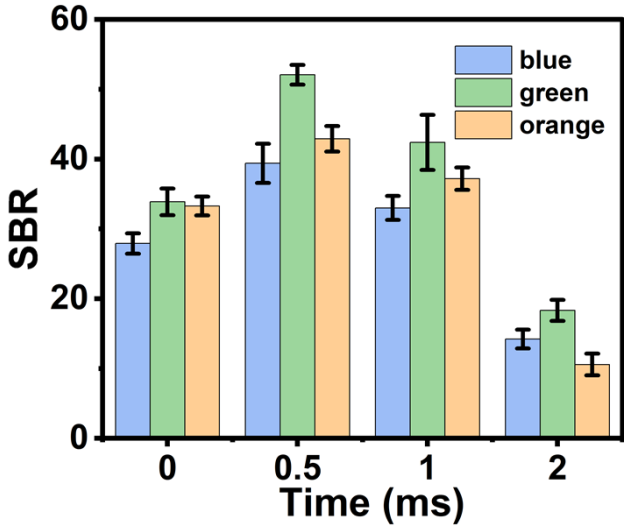

Figure S18. Statistical analysis of the signal-to-background ratio (SBR) of luminous intensity for different emission wavelengths at different delay times.

As displayed in Figure S18, the statistical analysis of the SBR of luminous intensity for 450 (blue, λ_{ex} = 405 nm), 550 (green, λ_{ex} = 515 nm) and 580 nm (orange, λ_{ex} = 515 nm) emission wavelengths at 0, 0.5, 1 and 2 ms delay times was performed. A long-lived phosphorescence signal with a lifetime of more than 2 ms can also be clearly detected at different emission fields. The SBR values for the blue, green and orange phosphorescent signals are 27.9, 33.9, and 33.3 at 0 ms; 39.4, 52.1, and 42.9 at 0.5 ms; 33.0, 42.4, and 37.2 at 1 ms; and 14.2, 18.3, and 10.6 at 2 ms, respectively.

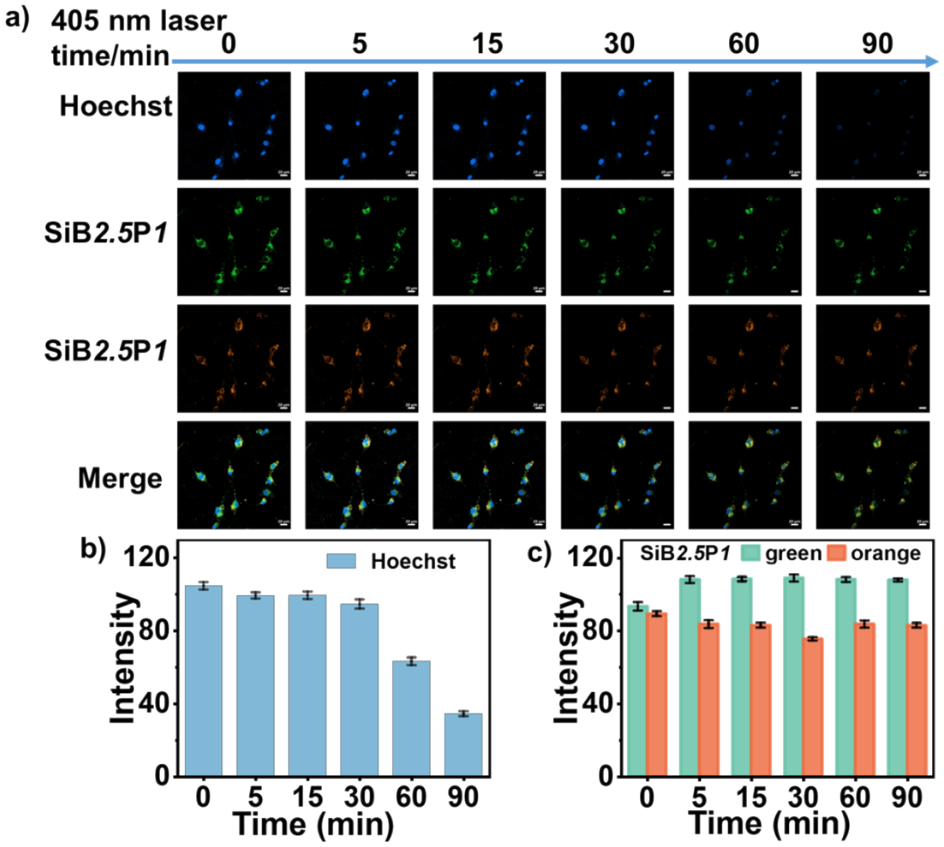

Figure S19. (a) Confocal images of U87 cells incubated with Hoechst blue fluorescence dye for nuclei and SiB*2.5*P*1* after continuous light for 0-90 min. Scale bar: 20 μm. Luminous intensity statistics of Hoechst (b) and SiB*2.5*P*1* (c) after continuous light exposure for 0-90 minutes.

As displayed in Figure S19, images are collected under a 405 nm laser at different light wavelengths (0-90 min). The intensity analysis of the images is performed with ImageJ 1.54d. Interestingly, the intensity of SiB*2.5*P*1* is essentially unchanged (Figure S19c); however, the intensity of the Hoechst dye decreases by more than a factor of 3, suggesting that SiB*2.5*P*1* exhibits excellent photostability in living cells.[8]

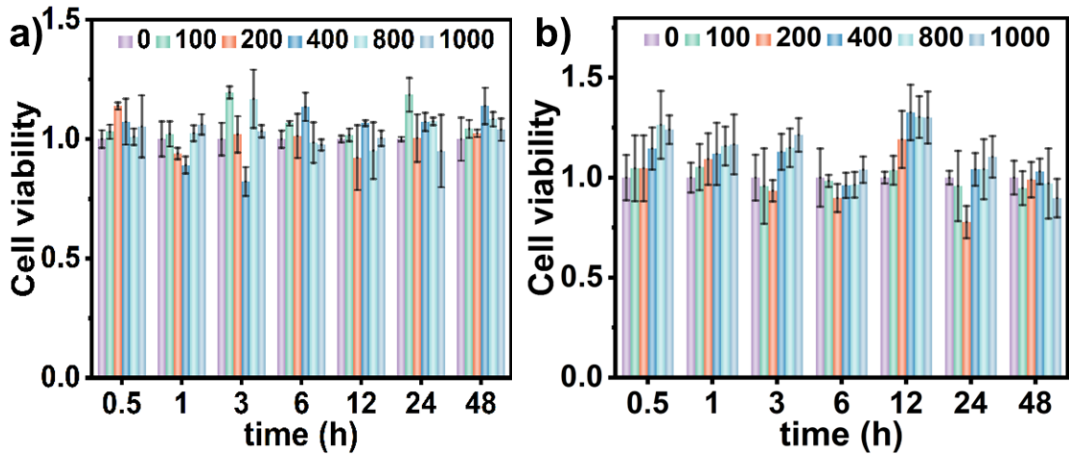

Figure S20. Cytotoxicity of SiB*2.5*P*1* toward (a) HBMEC and (b) U87 cells during 0.5-48 h of incubation at various concentrations (0-1000 μg/mL) (n = 6, mean±SD).

The viability of both HBMEC and U87 cells treated with SiB*2.5*P*1* at different concentrations (0-1000 μg/mL) is greater than 80% after 0.5-48 h of incubation. These results indicate that the as-prepared SiB*2.5*P*1* exhibits negligible cytotoxicity.

Table S1. Quantum yield of solid at different excitation wavelengths.

	320 nm	330 nm	340 nm	350 nm	360 nm	370 nm	380 nm	390 nm	400 nm
SiB*2*	0.065	0.126	0.201	0.258	0.301	0.3	0.224	0.169	0.142
SiB*2.5*	0.118	0.222	0.332	0.412	0.43	0.38	0.251	0.181	0.149
SiB*3*	0.131	0.228	0.325	0.393	0.387	0.32	0.209	0.16	0.139
SiB*2*.5P*0.5*	0.217	0.238	0.253	0.253	0.131	0.141	0.111	0.142	0.085
SiB*2.5*P*1*	0.035	0.057	0.089	0.133	0.164	0.095	0.089	0.105	0.126
SiB*2*.5P*2*	0.043	0.069	0.108	0.158	0.133	0.137	0.101	0.102	0.108

Table S2. Quantum yield in aqueous phase at different excitation wavelengths.

	320 nm	330 nm	340 nm	350 nm	360 nm	370 nm	380 nm	390 nm	400 nm
SiB*2*	0.058	0.097	0.128	0.133	0.159	0.139	0.118	0.076	0.063
SiB*2.5*	0.069	0.103	0.154	0.204	0.235	0.162	0.123	0.098	0.064
SiB*3*	0.076	0.108	0.147	0.192	0.183	0.142	0.102	0.074	0.059
SiB*2*.5P*0.5*	0.122	0.128	0.137	0.138	0.080	0.071	0.060	0.064	0.003
SiB*2.5*P*1*	0.028	0.045	0.068	0.111	0.127	0.041	0.053	0.062	0.071
SiB*2*.5P*2*	0.037	0.035	0.089	0.110	0.109	0.105	0.092	0.085	0.080

References

1. M. Cui, P. Dai, J. Ding, M. J. Li, R. Sun, X. Jiang, M. L. Wu, X. K. Pang, M. Z. Liu, Q. Zhao, B. Song and Y. He, *Angew. Chem. Int. Ed.*, 2022, **61**, e202200172.

2. X. Jiang, M. Wu, L. Zhang, J. Wang, M. Cui, J. Wang, X. Pang, B. Song and Y. He, *Anal. Chem.*, 2022, **94**, 7264-7271.
3. X. B. Shen, B. Song, B. Fang, A. R. Jiang, S. J. Ji and Y. He, *Chem. Commun.*, 2018, **54**, 4947-4950.
4. Z. Wang, Y. Liu, S. Zhen, X. Li, W. Zhang, X. Sun, B. Xu, X. Wang, Z. Gao and X. Meng, *Adv. Sci.*, 2020, **7**, 1902688.
5. P. Wei, X. Zhang, J. Liu, G. G. Shan, H. Zhang, J. Qi, W. Zhao, H. H. Sung, I. D. Williams, J. W. Y. Lam and B. Z. Tang, *Angew. Chem. Int. Ed.*, 2020, **59**, 9293-9298.
6. J. K. Li, X. Y. Chen, Y. L. Guo, X. C. Wang, A. C. Sue, X. Y. Cao and X. Y. Wang, *J. Am. Chem. Soc.*, 2021, **143**, 17958-17963.
7. H. Ma, Q. Peng, Z. An, W. Huang and Z. Shuai, *J. Am. Chem. Soc.*, 2019, **141**, 1010-1015.
8. T. Li, Y. Zhao, N. Zhang, K. Zhang, C. Zhang and T. F. Yi, *Adv. Funct. Mater.*, 2024, **34**, 2309663.